Journal of Materials Chemistry A

# The hetereostructured poly(3,6-dithien-2-yl-9H-carbazol-9-yl acetic acid)/TiO2 nanoparticles composite redox-active materials as both anode and cathode for high-performance symmetric supercapacitor applications



| | |
|---|---|
| Journal: | *Journal of Materials Chemistry A* |
| Manuscript ID: | TA-ART-01-2014-000109 |
| Article Type: | Paper |
| Date Submitted by the Author: | 07-Jan-2014 |
| Complete List of Authors: | GÜLLÜ, Mustafa; Ankara University, Chemistry<br>Yiğit, Deniz; Ankara University, Chemistry<br>Sınağ, Ali; Ankara University, Chemistry<br>Yumak, Tuğrul; Ankara University, Chemistry |
| | |

Journal of Materials Chemistry A

Cite this: DOI: 10.1039/c0xx00000x

www.rsc.org/xxxxxx

Full Paper

# The hetereostructured poly(3,6-dithien-2-yl-9H-carbazol-9-yl acetic acid)/$TiO_2$ nanoparticles composite redox-active materials as both anode and cathode for high-performance symmetric supercapacitor applications

**Deniz Yiğit,[a] Mustafa Güllü,*[a] Tuğrul Yumak,[a] and Ali Sınağ[a]**

***Received (in XXX, XXX) Xth XXXXXXXXX 20XX, Accepted Xth XXXXXXXXX 20XX***
**DOI: 10.1039/b000000x**

Herein, a facile and simple method was reported to prepare the composite electrode materials based on conducting polymer/nano metal oxide combination for supercapacitor applications. The hetereostructured composite redox-active electrode materials, having both p- and n-doping ability, were fabricated using poly(3,6-dithien-2-yl-9H-carbazol-9-yl acetic acid) and nano sized $TiO_2$ particles without any binder and conducting additives. The hetereostructured composite electrodes exhibited remarkable specific capacitance ($C_{spec}$= 462.88 F $g^{-1}$), specific power (SP= 266.96 kW $kg^{-1}$), specific energy (SE= 89.98 Wh $kg^{-1}$), good cycling performance and excellent reversible capability (81.7 % capacitance retention after 8000 charge/discharge cycles) at 2.5 mA $cm^{-2}$ current density within a 1.2 V potential window with two-electrode symmetric cell configuration. Besides, hetereostructured composite electrode materials were fabricated using different particle sized $TiO_2$ (3-5 nm, average 21nm and bulk), and effect of the particle size on supercapacitor performances were investigated and compared in detail. Our symmetric pseudo-capacitor device lighted a LED for 4.7 minutes with 42 seconds charge time at 2.5 mA $cm^{-2}$ even after 8000 charge/discharge cycles.

## 1. Introduction

Rapid development on fabrication of low-cost, lightweight and flexible advanced electronic systems such as digital communications devices, portable consumer electronic vehicles, standby high power systems and electric hybrid vehicles has generated considerable demand for alternative and efficient energy storage systems.[1-4] Supercapacitors have been the focus of scientists as new kind of electrical energy storage systems in order to meet this requirement. Supercapacitors fill the range between conventional dielectric capacitors and primary or secondary batteries in terms of their power (~15 kW $kg^{-1}$) and energy (~5 Wh $kg^{-1}$) densities and provide high power for a short time-period.[5] Compared to conventional energy storage devices, supercapacitors have many excellent advantages such as short charging times, long cycle life, high charge-storage efficiency, eco-friendlsy and safety primacies, as well as their relatively higher power densities.[6]

One of the most important component of a supercapacitor is its current collector so that the performance of supercapacitor depends strongly on the features of electroactive materials, such as electrical conductivity, internal resistance, surface porosity, thickness and durability. Therefore, recent researches in supercapacitor applications have mainly focused on development of new advanced electrode materials possessing high quality electrochemical and mechanical properties. Carbon-based materials such as carbon nanotubes (CNT), carbon nanofibers, graphenes and carbon aerogels have been regarded as very suitable electrode materials for supercapacitors due to their better active surface area and porosity, high charge mobility, excellent chemical and thermal stability, sufficient flexibility and mechanical strength.[7-11] Unfortunately, carbonaceous electrode materials deliver limited specific capacitances ($C_{spec}$) since they solely electrostatically store charge, similar to conventional physical capacitors, through a non-Faradaic process at the electrode/electrolyte interface. Moreover, carbon-based materials have higher internal resistance owing to the concact resistance of carbon particles, thus their supercapacitive performances have not yet reached the desired values.[12-15] On the other hand, π-conjugated organic polymers (electronically conducting polymers, CPs) and metal oxides have become the promising advanced electrode materials in terms of their higher $C_{spec}$, energy

and power densities. Because these redox-active materials store charge by fast and reversible redox reaction in addition to electrostatically charge accumulation and offer 10-1000 times greater $C_{spec}$ as compared to carbon-based electrode materials[16-22].

Up to date, certain metal oxides, $V_2O_5$, MoO, $SnO_2$, $IrO_2$, NiO, $MnO_2$, $TiO_2$ and $RuO_2$ have been used as redox-active electrode materials in pseudo-capacitor (PCs) applications and reported that they provide higher energy density[23-30]. But these materials suffer their higher internal resistance and poor electronic conductivity. These disadvantages are an obstacle to the capacitive performances of transition metal oxide-based PCs. Among metal oxide redox-active materials, although $RuO_2$-based electrode materials have exhibited pseudo-capacitance values as high as 200-900 F $g^{-1}$, it is not a suitable electrode material for practical or commercial supercapacitor applications due to its high cost. [31-34] By contrast to metal oxide-based electrode materials, CPs as redox-active materials show excellent electronic conductivity and higher power density in PC applications. Furthermore, they have fast switching properties between redox states, better mechanical flexibilities, excellent electrochemical reversibilities, lower fabrication cost and good environmental stability.[35-39] The PC devices fabricated by using π-conjugated polymers have demonstrated satisfactory capacitive performances and average $C_{spec}$ in the range of 100-500 F $g^{-1}$.[40-44] On the other hand, most of the π-conjugated polymer-based electrode materials can only be employed as anode material (positive redox-active electrode) against a different cathode material. This obligation is critical factor which increases internal resistance of PC devices and restricts pseudo-capacitive performances. A limited number of CPs such as poly(3,4-ethylenedioxythiophene) (pEDOT) are suitable for both positive (p-) and negative (n-) doping. Therefore, pEDOT-based symmetric supercapacitors have been extensively reported and shown $C_{spec}$ values in between 56 and 170 F $g^{-1}$.[21, 45-47] In our recent works, we have produced novel thiophene-based conducting polymers having both p- and n-doping ability, poly(thieno[3,4-b][1,4]dioxine) and poly(N-alkyl-3,4-dihydrothieno[3,4-b][1,4]oxazine) derivatives and observed $C_{spec}$ values (260, 285.6 and 325 F $g^{-1}$) better than pEDOT's.[48-49] CP-based redox-active materials usually have poor cycling stability compared to carbonaceous materials and transition metal oxides, which is thought to be an effect of swelling and shrinking of polymer backbone during doping/undoping process, causing generally a mechanical degradation on the surface of electrode material. Recently, hetereostructured composite electrode materials have been introduced in order to obtain better supercapacitive performances and to improve cycling stability of electrode materials. Single-wall carbon nanotubes (SWCNT), carbon nanofibers, carbon nanorods, conducting polymers and nano metal oxide particles including $MnO_2$, $SnO_2$, $V_2O_5$ and $NiFe_2O_4$ have been usually preferred in fabricating of composite electrodes because of their mechanical and electrochemical stability, mitigating mechanical stress properties, excellent electrochemical reversibilities, high power density and specific capacitance values, excellent large specific surface areas and highly porous structures.[50-56] For example, Liu *et al* have presented that cycling stability of pEDOT-based electrode materials can be increased by adding $RuO_2$ nanoparticles into conducting polymer matrix. The synergistic pseudo-capacitive effect of $RuO_2$ nanoparticles could also improve charge-storage capability of symmetric PC device constructed with pEDOT/$RuO_2$ hetereostructured composite electrode materials ($C_{spec}$= 1217 F $g^{-1}$).[57] Another study, by Bian *et al*, has indicated that fibriform polyaniline/nano-TiO2 composite electrode materials exhibited good capacitive performance ($C_{spec}$= 330 F $g^{-1}$) and electrochemical cycling stability (~ 92 % capacitance retention). [58] Carbon-based materials have also been modified by using nano metal oxide particles and their supercapacitive performances have been evaluated. Chen *et al* have fabricated free-standing and flexible three-dimensional graphene/carbon nanotubes/$MnO_2$ (3DG/CNTs/$MnO_2$) composite electrodes and maximum specific capacitance value of 343 F $g^{-1}$ and power density of 22 727.3 W $kg^{-1}$ have been obtained. [59] Three-dimensional ordered carbon nanotube (CNT)/polypyrrole (PPy) hetereostructured composite electrode materials were also prepared for supercapacitor applications. The supercapacitor cell constructed with CNT/PPy composite electrodes reached 427 F $g^{-1}$ specific capacitance and exhibited good galvanostatic charge/discharge stability after 1000 cycles.[60] The most important problem of hetereostructured composite electrode materials is the weak electrostatic interaction between nano metal oxide redox-active particles and conducting polymer backbone or carbon-based template materials. Many composite electrode materials suffer also another serious problem of agglomeration of metal oxide nanoparticles. To overcome weak interaction challenges and prepare highly dispersed composite materials, polymeric binders such as poly(tetrafluoroethylene) (PTFE) and poly(vinylidenefluoride) (PVDF) are generally used in the fabrication process of electrode materials. But, the presence of any binder in composition of composite electrode materials leads to a considerable rise in total cell resistance causing a limitation on both cycling stability/reversibility and capacitive performance, although it enables formation or a more homogeneous distribution.[61-63] Thus, cycling performances of many hetereostructured composite electrode materials based on conducting polymer/metal oxide are still not at a satisfactory level for long-term high performance supercapacitor applications. It clearly seems that feasible strategies, beyond the known methods, are extensively required in the combination of different redox-active materials in terms of developing new hetereostructured composite electrode materials with excellent cycling stability and capacitive performance.

In this context, the main motivation of this work is related to create practicable approaches for overcoming some disadvantages, above mentioned, including: *(i)* limitation of the number of conducting polymer-based redox-active electrode materials that can be used as both anode and cathode in pseudo-capacitor applications, *(ii)* the poor stability of the π-conjugated polymers/metal oxide composite materials caused by weak interaction between polymer chain and metal oxide, *(iii)* the aggregation problem of metal oxide redox-active particles in conducting polymer network. We proposed a rational and feasible method to prepare an example of a high-performance

hetereostructured composite electrode materials based on π-conjugated polymer and nano metal oxide. A carbazole unit-containing thiophene derivative, namely poly(3,6-dithien-2-yl-9H-carbazol-9-yl acetic acid) (pTCAA), in composition of our hetereostructured electrodes was purposefully designed to improve charge-storage behaviour and cyclic performance of the conducting polymer material. In this method, a strong chemical interaction between pendant carboxylic acid groups available on pTCAA backbone and transition nano-metal oxide particles, unlike electrostatic interaction, is expected for the construction of a much stronger pTCAA/$TiO_2$ hetereostructured. Thus, we aimed not only to increase cycling life and stability of the hetereostructured composite electrode materials, but also to generate more homogeneous conducting polymer/nano metal oxide particles composite matrix without binder, as well as improving capacitive performance. Nanoscaled $TiO_2$ particles was preferred to modify pTCAA polymer coated electrodes because of they can be prepared easily, economically and eco-friendly, relatively, compared to other metal oxides. Capacitive performances of symmetric PC devices constructed using the hetereostructured pTCAA/$TiO_2$ composite electrodes as both anode and cathode were evaluated by cyclic voltammetry (CV), galvanostatic charge/discharge (GCD) and electrochemical impedance spectroscopy (EIS) technique in the two electrodes configuration with organic electrolyte. Besides, hetereostructured pTCAA/$TiO_2$ composite electrode materials were fabricated using different particle sized $TiO_2$ (3-5 nm, average 21 nm and bulk) and effects of the particles size on supercapacitor performances of the electrodes were investigated and compared in detail.

## 2. Experimental

### 2.1 Materials

All chemicals were purchased from Sigma Aldrich and used without any further purification. Average 21 nm $TiO_2$ (average 21 nm particle size, Degussa P25) and bulk $TiO_2$ particles were purchased from Evonik Industries and Fisher Scientific, respectively. Stainless steel (99.9%, SS) was commercially obtained and used as current collector substrate in dimensions of 10 mm width, 10 mm length and 0.4 mm thickness. 3,6-Dibromo-9H-carbazole was synthesized according to previously described method.[64] Prior to electrochemical studies, acetonitrile (ACN) was refluxed with $P_2O_5$ for 6 h, then distilled fractionally and stored over activated 4A molecular sieves. Tetrabutylammonium tetrafluoroborate ($Bu_4NBF_4$) was dried at 90º C for 12 h prior to use. The $Ag/Ag^+$ pseudoreference silver wire electrode was calibrated using the $Fc/Fc^+$ redox couple standart (0.21 V *vs* silver wire).

### 2.2 Synthesis of monomer

The target thiophene/carbazole monomer was synthesized in three steps as explained below.

**Ethyl (3,6-dibromo-9H-carbazol-9-yl)acetate (2a)**

In a dry 100 mL two-necked round-bottomed flask, 3,6-dibromo-9H-carbazole **(1a)** (325 mg, 1mmol) and anhydrous $K_2CO_3$ (276 mg, 2mmol) was suspended in dry DMF (25 mL). Then, ethyl chloroacetate (146.5 mg, 1.2 mmol) was added dropwise to the suspension at room temperature. The reaction mixture was stirred and heated at 110º C overnight under nitrogen atmosphere. The reaction mixture was poured into ice-water (100 mL) and the aqueous layer was extracted with chloroform (3 x 25 mL). The combined organic phase was washed by water and brine, dried over anhydrous $Na_2SO_4$. The solvent was removed on a rotary evaporator under reduced pressure. The residual solid product was recrystallized from ethanol/water (1:1) mixture to afford **2a** (357.5 mg, 0.87 mmol, 87%, mp 178-180ºC) as a white powder. FTIR ν/$cm^{-1}$ 3081, 3062, 2980, 2916, 1735, 1595, 1473, 1438, 1366, 1348, 1290, 1232, 1209, 1151, 1053, 1008, 831. $^1$H NMR (400 MHz, $CDCl_3$, $Me_4Si$) $\delta_H$ 1.24 (t, *J*=7.2, 3H), 4.21 (q, *J*= 7.2, 2H), 4.95 (s, 2H), 7.2-7.22 (d, *J*=8.8, 2H), 7.55-7.58 (dd, *J*=6.5 and *J*=2, 2H), 8.15 (d, *J*=1.6, 2H) MS (EI): *m/z* 411 ($M^+$).

**Ethyl (3,6-dithien-2-yl-9H-carbazol-9-yl)acetate (3a)**

In a dry 50 mL three necked round-bottomed flask fitted with a condenser and argon inlet, ethyl (3,6-dibromo-9H-carbazol-9-yl)acetate **(2a)** (616.5 mg, 1.5 mmol) and 2-(tributylstannyl)thiophene **(4) (**1678.5 mg, 4.5 mmol**)** were dissolved in dry DMF (15 mL). The solution was intensely purged with argon at room temperature for 15 min and bis(triphenylphosphine)palladium (II) dichloride ($PdCl_2(PPh_3)_2$, 17.5 mg, 0.025 mmol) was added. The reaction mixture was heated at 100º C for 24 h under argon atmosphere, cooled, and poured into water (50 mL). The aqueous layer was washed with saturated KF solution, extracted with chloroform (3 x 30 mL), and dried over sodium sulphate. After removal of chloroform by evaporation under reduced pressure, the crude product was purified by column chromatography using $SiO_2$ as solid phase and hexane/ethyl acetate (3:1 v/v) as eluent ($R_f$, 0.45) afforded **3a** (575 mg, 1.38 mmol, 92%, mp 153-155º C) as a bright brown solid. FTIR ν/$cm^{-1}$ 3076, 2985, 2919, 2852, 1735, 1592, 1475, 1430, 1364, 1345, 1287, 1230, 1200, 1155, 1050, 1028, 875. $^1$H NMR (400 MHz, $CDCl_3$, $Me_4Si$) $\delta_H$ 1.24 (t, *J*=7.2, 3H), 4.22 (q, *J*=7.2, 2H), 5 (s, 2H), 7.11-7.13 (dd, *J*=8.2 and *J*=3.2, 2H), 7.27-7.29 (dd, *J*=6 and *J*=1.2, 2H), 7.32-7.34 (d, *J*=8.8, 2H), 7.35-7.37 (dd, *J*=4.4 and *J*=1.2, 2H), 7.75-7.73 (dd, *J*=6.6 and *J*=2, 2H), 8.34 (d, *J*=1.6, 2H). MS (EI): *m/z* 417 ($M^+$).

**3,6-Dithien-2-yl-9H-carbazol-9-yl acetic acid (TCAA)**

KOH (72.5 mg, 85%, 1.1 mmol) was dissolved in 3 mL $H_2O$/ 9 mL EtOH mixture. **3a** (417 mg, 1mmol) was added to this basic solution, and the reaction mixture was refluxed for 5 h. The reaction content was cooled to room temperature, extracted with ether to remove unreacted ester first, and poured into ice-water mixture (20 mL). The basic aqueous phase was acidified with 37% HCl to pH 3-4. The solid product was filtered under reduced pressure, dried and recrystallized from methanol/water (1:3) to afford **TCAA** (377 mg, 0.97 mmol, 97%, mp 292º C (decomp.)) as a light green solid. FTIR ν/$cm^{-1}$ 3519-2166, 3109, 3071, 2952-2852, 1707, 1604, 1588, 1483, 1420-1352, 1290, 1235, 1211, 1078, 1047, 957, 878, 821. $^1$H NMR (400 MHz, $CDCl_3$, $Me_4Si$) $\delta_H$ 5.24 (s, 2H), 7.13-7.15 (dd, J=8.4 and J=3.6, 2H), 7.47-7.49 (dd, J=6 and J=0.8, 2H), 7.53-7.54 (dd, J=4.8 and J=1.2, 2H),

7.57-7.59 (d, J=8.4, 2H), 7.73-7.75 (dd, J=8.7 and J=1.6, 2H), 8.57 (d, J=1.6, 2H). $^{13}$C NMR (400 MHz, DMSO, $Me_4Si$) $\delta_C$ 44.2, 110.5, 118, 122.97, 123.26, 124.64, 124.84, 126.15, 128.83, 141, 145.12, 170. MS (EI): *m/z* 389 ($M^+$). Anal. Calcd. for ($C_{22}H_{15}NO_2S_2$): C, 67.84%; H, 3.88%; N, 3.60%. Found: C, 67.63%; H, 3.70%; N, 3.47%.

### 2.3 Synthesis of $TiO_2$ nanoparticles (3-5 nm)

3-5 nm nanosized $TiO_2$ particles were hydrothermally synthesized according to previously reported and well characterized by transmission electron microscopy (TEM), scanning electron microscopy (SEM), Brunauer-Emmett-Teller (BET) and X-ray diffaraction (XRD) methods.[65]

### 2.4 Preparation of hetereostructured pTCAA/$TiO_2$ composite electrode materials

Electrochemical redox behaviour of 3,6-dithien-2-yl-9H-carbazol-9-yl acetic acid (TCAA) was firstly determined by using CV in order to understand oxidation-polymerisation behaviour of the monomer and prepare hetereostructured composite electrode materials accordingly. CV study was performed using a three-electrode cell configuration including platinum wire working electrode and platinum wire counter electrode against a $Ag/Ag^+$ pseudoreference silver wire electrode in a potential range 0 – 2.0 V *vs* $Ag/Ag^+$ at a scan rate of 150 mV $s^{-1}$. The results of CV indicated that TCAA exhibited irreversible oxidation peak at + 1.95 V. Immediately after the oxidation of monomer, polymer film rapidly formed on platinum working electrode with an increase in the current density. Oxidation peak of poly(3,6-dithien-2-yl-9H-carbazol-9-yl acetic acid) (pTCAA) was also observed at + 1.42 V after 2$^{nd}$ and 3$^{rd}$ cycles in the cyclic voltammograms as shown in **Fig. S8**† (see EIS†).

Following the determination of electrochemical oxidation potentials of novel thiophene/carbazole based monomer (TCAA) and its conducting polymer, pTCAA coated stainless steel (SS) substrates were prepared by the constant potential electrolysis. Electrolyses were carried out at + 1.45 V in the presence of 0.03 M monomer in 0.1 M $Bu_4NBF_4$/ACN under nitrogen atmosphere with a charge density of 250 mC $cm^{-2}$ for 1.5 min, using platinum auxiliary electrode and $Ag/Ag^+$ pseudoreference electrode. After deposition of the electroactive polymer films, the polymer coated SS substrates were rinsed with ACN in order to remove the supporting electrolyte and unreacted monomer. Then, the SS substrates coated polymer films were kept in an oven at 65º C for 6 h to remove the solvent. FTIR ν/$cm^{-1}$ 3360-2250, 3080, 2945, 1710, 1640, 1508, 1425, 1319, 1284, 1223, 1156, 1080, 876. Anal. Calcd. for $(C_{22}H_{13}NO_2S_2)_n$: C, 68.02%; H, 3.63%; N, 3.61%. Found: C, 67.66%; H, 3.48%; N, 3.49%.

Finally, pTCAA conducting polymer films were modified with $TiO_2$ nanoparticles (3-5 nm, average 21 nm and bulk) to construct hetereostructured pTCAA/$TiO_2$ composite electrode materials. For a typical modification process of electrode materials, 5 mM ethanol suspension of $TiO_2$ particles was firstly prepared under sonication conditions and pTCAA coated SS substrates was immersed into this suspension for 12 h. After loading of $TiO_2$ nanoparticles, hetereostructured pTCAA/$TiO_2$ composite electrode material was rinsed with ethanol and acetone, and dried in a nitrogen atmosphere. The mass of redox-active material deposited on SS substrate was weighed out using a microanalytical balance (Δm=± 0.001 mg) four times in a row. The average of four measurements was used as active material mass in electrochemical measurements.

### 2.5 Characterization of materials

The chemical structure of TCAA was characterized by $^1$H NMR, $^{13}$C NMR, FTIR, mass spectroscopy and elemental analysis, while its polymer, pTCAA, was characterized by FTIR, scanning electron microscopy (SEM) and elemental analysis after undoping of $BF_4^-$ anions cathodically (-0.3 V). The characterization of hetereostructured pTCAA/$TiO_2$ composite electrode materials were conducted with scanning electron microscopy (SEM, Zeiss Ultra Plus FE-SEM and Zeiss Evo 40 500V-30kV) and X-ray diffraction (XRD, Rigaku D/Max-2200 ULTIMAN). $^1$H NMR and $^{13}$C NMR spectra were recorded at room temperature on Varian-Mercury 400-MHz high performance digital Fourrier-transform (FT) NMR spectrometer with tetramethyl silane (TMS) as an internal standart. All chemical shifts were given in ppm. FTIR spectra were recorded on a Perkin-Elmer Spectrum 100 spectrometer. Mass spectra were recorded with Agilent Technologies 6890N Network GC System and Agilent Technologies 5975B VL MSD operating and Shimadzu GC-MS QP2010 mass spsctrometer (DI-2010 direct inlet probe) at an inoization potential (EI) of 70 eV. Elemental analyses for C, H and N were performed with a Eurovector CHNS Elemental Analyser.

### 2.6 Assembly of pseudo-capacitor (PC) devices

The symmetric type different symmetric PC devices (*Type I-III*) and symmetric type reference PC device (*Type IV*) were constructed by using hetereostructured pTCAA/$TiO_2$ composite electrode materials and only pTCAA coated SS electrodes, respectively, in this work. For assembly of PC devices, 0.5 M $Bu_4NBF_4$/ACN supporting electrolyte solution was firstly dropped to composite electrode surface until fully wetted. Then, thin separator paper soaked to 0.5 M $Bu_4NBF_4$/ACN supporting electrolyte solution was placed between the anode and cathode to prevent contact with electrodes. Finally, PC devices was hermetically sealed by using paraffin band. A two-electrode system configuration was set up by connecting reference electrode on the side of auxiliary electrode for the devices. As an example for symmetric PC device is represented in **Fig. S9**† (see EIS†).

### 2.7 Capacitive performance tests of PC devices

Cyclic voltammetry (CV), galvanostatic charge/discharge (GCD) and electrochemical impedance spectroscopy (EIS) techniques were employed for supercapacitive performance tests of all symmetric PC devices. The electrochemical performance tests were carried out with two-electrode cell configuration under ambient conditions. CV studies were performed in between 0.0 V and + 1.2 V potential range at various scan rate (5, 10, 25, 50, 100, 150 and 250 mV $s^{-1}$). GCD tests for PC devices were carried

out at 2.5, 5, 7.5 and 10 mA $cm^{-2}$ constant current densities in between 0.0 V and +1.2 V potential range. Stability tests of the PC devices were performed by using galvanostatic charge/discharge technique at 2.5 mA $cm^{-2}$ constant current density within 1.2 V potential window over 8000 cycles. The impedance plots were recorded using an amplitude of 5 mV rms in a frequency range from $10^4$ to 0.01 Hz at applied DC voltage of 0 V. CV and EIS studies were carried out by using a PAR (Princeton Applied Research) 2273 potensiostat/galvanostat computer-controlled using PowerSuite software program. GCD tests of PC devices were performed with a Radiometer VoltaLab PST050 Potensiostat/galvanostat-High Voltage Booster 100 V HVB100. Equivalent circuit modelling studies were performed using experimental impedance data with the aid of ZSimpWin 3.50 commercial software according to a complex nonlinear least-squares (CNLS) method.

## 3. Results and discussion

In this work, a new kind of hetereostructured composite electrode material was aimed and designed for supercapacitor applications. Conducting polymer part of the current collector was specifically designed by taking into consideration of a charge storage mechanism of a conducting polymer as a redox-active material as well as its carboxylic acid functional group in binding $TiO_2$ nanoparticles. It is well known that carbazole derivatives have high charge carrier capability, conveience of formation of stable radicals and good hole transporting ability. Regarding to these distinctive features, carbazole based conducting polymers generate polarons and/or bipolarons on the polymer backbone, more effective and stable.[66-68] The polaronic species are the basis of pseudo-capacitance phenomenon for a conducting polymer.[3] Therefore, a carbazole based monomer was especially chosen in this study in order to increase charge/discharge efficiency and stability of our polymeric redox-active material during Faradaic charge/discharge process. Additionally, an acetic acid moiety was desired to be attached to the carbazole ring from nitrogen atom in order to get better bonding between conducting polymer and metal oxide particles.

Synthesis of the designed thiophene/carbazole-based novel monomer, namely, 3,6-dithien-2-yl-9H-carbazol-9-yl acetic acid (TCAA), was prepared initially to produce required hetereostructured composite electrode materials. As illustrated in Scheme 1, TCAA was obtained in excellent yield for the first time according to three-step synthetic methodology and its chemical structure was confirmed by FTIR, $^1$H NMR, $^{13}$C NMR, mass spectroscopy and elemental analysis techniques.

Subsequently, determination of electrochemical behaviour and oxidation potential of TCAA were performed by CV, which indicated that TCAA is an electroactive and oxidized at +1.95 V. Conducting polymer coated SS substrate were then prepared by constant potential electrolysis of the monomer at oxidation peak potential. Thin pTCAA polymer films deposited onto SS surfaces were characterized by FTIR, SEM and elemental analysis. In FTIR spectrum of pTCAA, seemed to be different from FTIR spectrum of monomer (TCAA), distinctive absorption bands present at around 1640 $cm^{-1}$ and 1080 $cm^{-1}$. The former can be attributed to polyconjugation, while the latter belongs to $BF_4^-$ anions doped into pTCAA polymer chain during electropolymerization process. These evidences prove the formation of conducting polymer film and n-doping process.

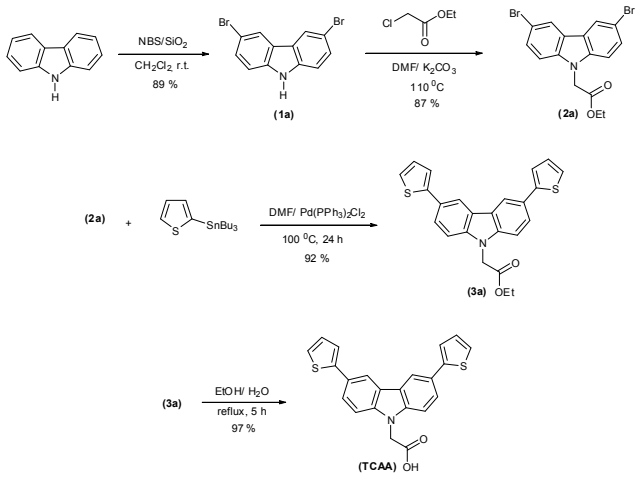


**Scheme 1** Synthetic route for TCAA

SEM images also contribute to the formation conducting polymer layer on SS substrate surfaces. As shown in **Fig. S10a†** (see EIS†), the surface morphology of raw SS substrate has a highly smoothly ordered structure. On the other hand, **Fig. 2a** clearly depicts that pTCAA polymer film brought forth a characteristic cauliflower-like appearance over the entire SS surfaces.

Following anodic electrodeposition process of thin polymeric film, the polymer coated SS substrates were successfully modified with nanosized $TiO_2$ particles. In the modification process, a novel strategy which has been not used to prepare conducting polymer based composite electrodes for pseudo-capacitors up to now, was employed in order to fabricate hetereostructured pTCAA/$TiO_2$ composite electrode materials. Different from an electrostatic interaction, $TiO_2$ nanoparticles were bound to conducting polymer surface *via* a strong interaction between pendant carboxylic acid groups on pTCAA backbone and transition nano-metal oxide particles. As well known, the carboxylic acid groups form a strong bond with titanium ions in this type interactions.[69-70] It may be suggested that such an interaction may not only further improve synergistic pseudo-capacitive behaviour but also increase the stability of hetereostructured composite redox-active materials (**Fig. 1**). Additionally, in the modification process of pTCAA coated SS electrodes, various particle sized $TiO_2$ nanoparticles such as 3-5 nm, average 21 nm and bulk scaled were used in order to investigate the effect of transition metal oxide particle size on capacitive performance of novel electrode materials.

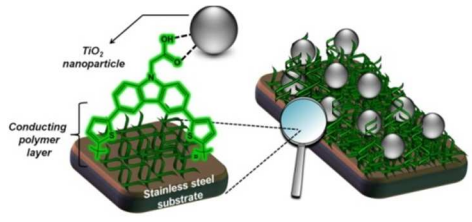


**Fig.1** Schematic representation of hetereostructured pTCAA/$TiO_2$ composite electrode material

The hetereostructured pTCAA/$TiO_2$ composite electrodes were

characterized by means of SEM and XRD and results were found to be satisfactory. As shown in **Fig. 2b**, **Fig. 2c** and **Fig. 2d**, the SEM images display that each hetereostructured pTCAA/$TiO_2$ composite redox-active electrode material has very porous three-dimensional surface morphology which is thought to be an appropriate surface morphology for supercapacitor applications.

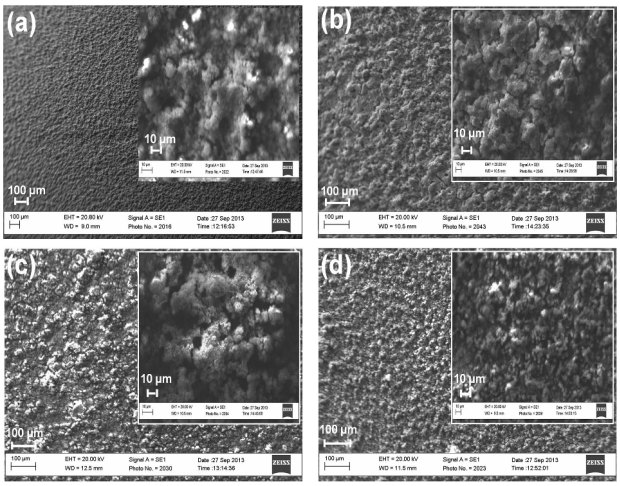


**Fig.2** SEM images of (a) pure polymer coated SS electrode (b) pTCAA/$TiO_2$ (3-5 nm) (c) pTCAA/$TiO_2$ (21 nm) (d) pTCAA/$TiO_2$ (bulk) hetereostructured composite electrode materials (insets are the corresponding magnified SEM images)

**Fig. S12a-c**† show the XRD patterns of the hetereostructured composite electrode materials. For all the pTCAA/$TiO_2$ composite materials, the two characteristic peaks at $2\theta \approx 25^{o}$ and 48º, corresponding to (101) and (200) diffraction peaks of $TiO_2$, were clearly observed in XRD patterns. All XRD reflections of $TiO_2$ nanoparticles in composition of hetereostructured electrode materials can be indexed to the reflections of anatase phase of $TiO_2$ (JCPDS card No. 84-1286). The sharp and clear diffraction peaks in XRD patterns also indicate that modification process of conducting polymer redox-active layer with metal oxide particles has no distinguishable effect on the crystallinity of $TiO_2$ nanoparticles in spite of strong interaction between pTCAA backbone and transition nano-metal oxide particles. On the other hand, peaks of pTCAA polymeric material are hardly detected from XRD patterns of the hetereostructured pTCAA/$TiO_2$ composite electrode materials since the crystal structure of $TiO_2$ particles represses the amorphous structure of pTCAA with low intensity and broad pattern, as expected. The results of XRD analysis confirm the success of novel modification strategy used in preparation of the hetereostructured pTCAA/$TiO_2$ composite electrode materials.

Symmetric type three different PC devices were assembled to test electrochemical performances of hetereostructured pTCAA/$TiO_2$ composite redox-active electrode materials. The hetereostructured pTCAA/$TiO_{2\ (3\text{-}5\ nm\ sized)}$, pTCAA/$TiO_{2\ (21\ nm\ sized)}$ and pTCAA/$TiO_{2\ (bulk\ sized)}$ electrodes were used as both p-dopable (anode) and n-dopable (cathode) electrodes to construct *Type I*, *Type II* and *Type III* PC devices, respectively. Besides, a symmetric type reference PC devices (*Type IV*) was also fabricated using pure pTCAA coated SS electrodes for comparison the capacitive performances of PC devices and evidently understanding the effect of metal oxide particle size on supercapacitive behaviours. A typical two-electrode configuration was preferred for all electrochemical performance tests owing to its obvious advantages, in this study. Unlike three-electrode configuration, the potential difference applied to cell is equally shared by working electrode and auxiliary electrode in two-electrode configuration. This means that electric charges are transferred out of both electrodes and the supercapacitive parameters such as specific capacitance, specific power and energy are calculated based on the entire cell. Moreover, two-electrode configuration systems can be easily adapted to practical and commercial applications.

Electrochemical performances of PC devices were investigated by cyclic voltammetry (CV), galvanostatic charge/discharge (GCD) and electrochemical impedance spectroscopy (EIS) techniques. In order to evaluate current-potential responses and supercapacitive behaviours of PC devices, initially, CV tests were performed in between 0.0 V and +1.2 V potential range which is ideal working potential window determined for our PC devices, at 5, 10, 25, 50, 100, 150 and 250 mV $s^{-1}$ scan rates. As shown in **Fig. 3a-d**, all of the CV curves exhibited close to nearly rectangular shaped and mirror-image current-potential profiles. No obvious deviation from rectangularity in the CV profiles was observed as the scan rate increased from 5 to 250 mV $s^{-1}$. The noteworthy characteristic responses mean that each of our hetereostructured pTCAA/$TiO_2$ composite electrode has an ideal supercapacitive behaviour and high-rate reversibility and stability during Faradaic charge/discharge process. CV studies also manifested synergistic pseudo-capacitive effect of $TiO_2$ nanoparticles. As can be seen in **Fig. 3e**, the normalized areas of the CV curves of *Type I*, *Type II* and *Type III* PC devices under the same scan rate of 100 mV $s^{-1}$ are broader than *Type IV*'s. There is an increase of 1.92-fold, 1.7-fold and 1.54-fold in capacitive current of *Type I*, *Type II* and *Type III* PC devices, respectively, compared to *Type IV*, so nanosized $TiO_2$ redox-active layer on the conducting polymer surface provides extra pseudo-capacitance. On the basis of CV results, it can be also proposed that capacitive performances of the hetereostructured pTCAA/TiO2 composite electrode materials fabricated using 3-5 nm sized $TiO_2$ particles outperform others (average 21 nm and bulk $TiO_2$).

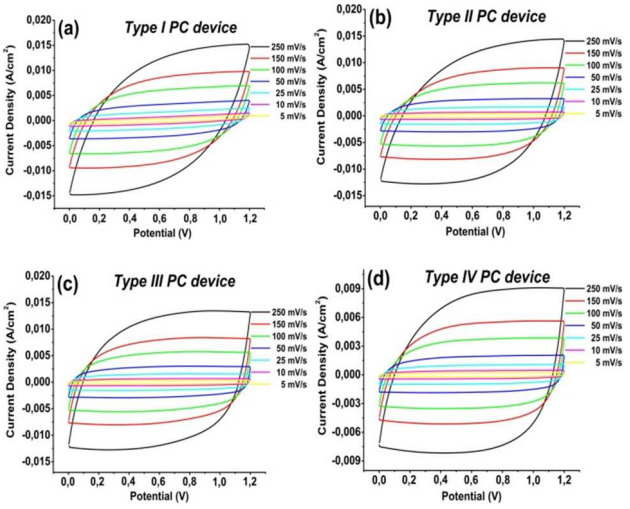

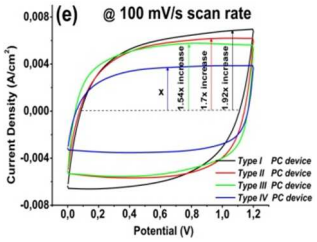


**Fig.3** Cyclic voltammograms of (a) *Type I* (b) *Type II* (c) *Type III* and (d) *Type IV* symmetric PC devices at different scan rates (e) comparative cyclic voltammograms of PC devices at 100 mV $s^{-1}$

The supercapacitive performances of PC devices were further examined by GCD technique with a potential window from 0.0 V to +1.2 V, corresponding to potential range obtained in CV studies, at various constant current densities (2.5, 5, 7.5 and 10 mA $cm^{-2}$). GCD measurements are essential in calculation of important parameters such as specific capacitance ($C_{spec}$), specific energy (SE) and charge/discharge efficiency (η) for practical supercapacitor applications. Typical GCD curves of symmetric PC devices at different constant current densities and the comparison of GCD curves of all PC devices at a constant current density of 2.5 mA $cm^{-2}$ are given in **Fig. 4a-e**. Our symmetric PC devices exhibited nearly triangle-like GCD profile, which is anticipated good charge/discharge behaviour and excellent reversible redox reaction for an ideal supercapacitor. Additionally, ohmic (*IR*) drop values were observed to be very small as 0.098 V, 0.11 V, 0.08 V and 0.085 V for *Type I*, *Type II*, *Type III* and *Type IV* PC device, respectively, at the same constant current density of 2.5 mA $cm^{-2}$. This indicates that hetereostructured pTCAA/$TiO_2$ composite and pure pTCAA coated SS electrode materials have fairly well electrical conductivities and low internal resistance, which are crucial parameters in terms of a better capacitive performance and high cycling stability. Using the galvanostatic charge/discharge curves at 2.5 mA $cm^{-2}$ current density, the specific capacitance values ($C_{spec}$, F $g^{-1}$) of our PC devices were calculated based on the following equation:

$$C_{spec} = (i \times t_d) / (\Delta V \times m_{ac}) \quad (1)$$

where $i$ is the discharge current (mA $cm^{-2}$), td is the discharge time (s), ΔV is the potential difference (V) in the discharge process and $m_{ac}$ is the total mass of active material in the electrodes.

As seen in Table 1, *Type I* (462.88 F $g^{-1}$), *Type II* (389.23 F$g^{-1}$) and *Type III* (357.65 F $g^{-1}$) PC symmetric devices delivered higher specific capacitances than *Type IV* (222.79 F $g^{-1}$) reference PC device. These differences in charge-storage capabilities of PC devices reveal the synergistic pseudo-capacitive effect of two different redox-active materials, just as obtained from CV results. The relatively higher specific capacitance value of *Type I PC* device may be attributed to formation of a more efficient and a more porous three-dimensional redox-active layer by 3-5 nm sized $TiO_2$ particles on hetereostructured electrode surfaces so as this provided a better Faradaic charge transfer process, compared to average 21 nm and bulk $TiO_2$ particles. As it is well known, the specific capacitance tends to a remarkable decrease with increasing charge/discharge current density since redox reactions and the diffusion rates of electrolyte ions are very low at high constant current densities. On the other hand, *Type I*, *Type II* and *Type III* PC devices were still able to retain 82.78% (from 462.88 to 383.14 F $g^{-1}$), 85.76% (from 389.23 to 333.78 F $g^{-1}$) and 87.47% (from 357.65 to 312.82 F $g^{-1}$) of their initial specific capacitance values, respectively. These results demonstrated that hetereostructured pTCAA/$TiO_2$ composite electrode materials have high charge/discharge rates even at high current density.

Charge/discharge or Coulombic efficiency (η) and specific energy (SE) are important parameters for supercapacitor applications and they can easily be evaluated using GCD curves. These values, summarized in Table 1, were calculated from GCD curves at 2.5 mA $cm^{-2}$ current density according to the following equations for our PC devices.

$$\eta = (t_d / t_c) \times 100 \quad (2)$$

$$SE = (C_{spec} \times (\Delta V)^2) / 2 \quad (3)$$

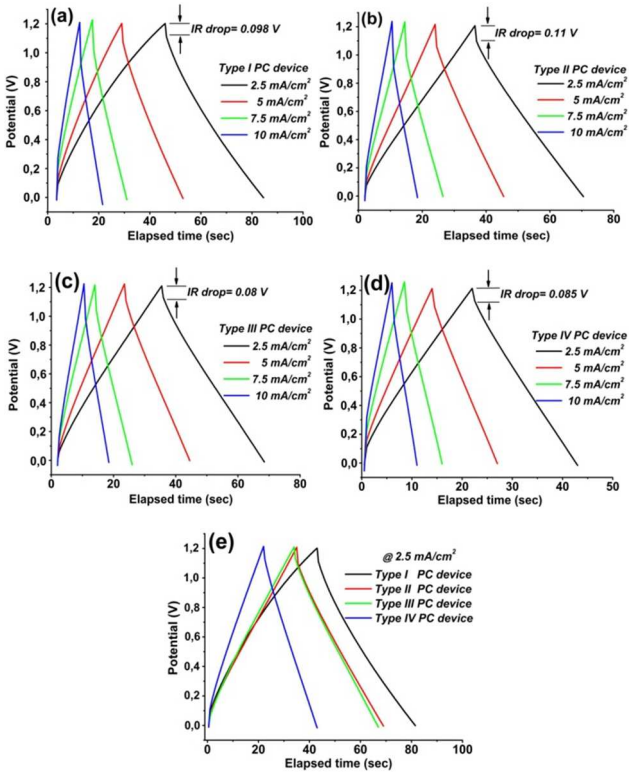


**Fig.4** Typical GCD curves of (a) *Type I* (b) *Type II* (c) *Type III* (d) *Type IV* symmetric PC devices at different current densities (e) the comparative GCD curves of all PC devices at 2.5 mA $cm^{-2}$ constant current density (f) the cycling performances of PC devices at a discharge current density of 2.5 mA $cm^{-2}$ for 8000 charge/discharge cycles

Where $t_d$ is the discharge time (s), $t_c$ is the charge time (s), $C_{spec}$ is the specific capacitance of the cell and ΔV is the potential difference (V) in the discharge process. PC devices exhibited both good charge/discharge reversibilities with close to 100 % Coulombic efficiencies and gratifying specific energy values as high as 89.98, 75.66 and 69.52 W h $kg^{-1}$ for *Type I*, *Type II* and *Type III* respectively. Specific energy and capacitance values of our hetereostructured pTCAA/$TiO_2$ composite electrode materials

are higher as compared to other composite electrodes based on $TiO_2$ nanoparticles reported in the literature.[58-60, 71-77]

A pseudo-capacitor device should have high rate cycling stability for long-term practical applications. Hence, we also examined cycling stabilities of our PC devices using galvanostatic charge/discharge procedure at 2.5 mA $cm^{-2}$ current density in the potential range between 0.0 V and +1.2 V for 8000 cycles in order to determine the utilizable limit of the hetereostructured pTCAA/$TiO_2$ composite electrode materials. The specific capacitance changes of PC devices as a function of cycle number, also known as the cycle-life plot, are presented in **Fig. 4f**. *Type IV* reference PC device retained only 51.2 % of its initial specific capacitance value (from 222.79 to 114.06 F $g^{-1}$) due to conducting polymer surface degradation during the long-term charge/discharge study. In contrast, *Type I*, *Type II* and *Type III* PC devices managed to retain 81.7 % (from 462.88 to 378.17 F $g^{-1}$), 79.3 % (from 389.23 to 308.65 F $g^{-1}$) and 77.5 % (from 357.65 to 277.17 F $g^{-1}$) of their initial specific capacitance values, respectively, by the end of 8000 charge/discharge cycles in stability tests. These high rate performances are clearly indicated that synergistic effect of $TiO_2$ redox-active layer prevented deformation of the conducting polymer surface, as well as its extra pseudo-capacitance. The results of long-term stability tests also confirmed the success and applicability of our rational methodology designed to improve cycling stability and reversibility of the hetereostructured composite electrode materials.

**Table 1** Specific capacitance, specific energy, specific power values and Coulombic efficiencies of PC devices.

| *PC device* | *Specific capacitance ($C_{spec}$) (F/g)** | *Coulombic efficiency (η) (%)* | *Specific Energy (SE) (W h/kg)* | *Specific Power (SP) (kW/kg)* |
|---|---|---|---|---|
| *Type I* | *462.88* | *94.51* | *89.98* | *266.96* |
| *Type II* | *389.23* | *99.07* | *75.66* | *202.59* |
| *Type III* | *357.65* | *98.09* | *69.52* | *138.89* |
| *Type IV* | *222.79* | *97.21* | *43.31* | *104.59* |

* *$C_{spec}$ values were calculated by using charge/discharge curves at 2.5 mA $cm^{-2}$ constant current density. IR drop levels were taken into account in $C_{spec}$, SE and SP measurements.*

Electrochemical impedance spectroscopy (EIS) was employed to evaluate internal resistances, charge transfer kinetics and ion diffusion rates of symmetric PC devices. The impedance spectra, as known Nyquist plots, of PC devices are given in **Fig. 5a-d**. A typical supercapacitor's Nyquist plot consists of a semi-circle pattern in high frequency region and a linear portion over low frequency region. The semi-circle defines electron transfer kinetic at the electrode material-electrolyte interface during redox reaction, while the linear portion is descriptive of ionic mass diffusion or transportion process. As shown in **Fig 5a-d**, all our PC devices exhibited small diameter semi-circle patterns which attributed to relatively low charge transfer resistances ($R_{CT}$) resulting from interaction between redox-active electrode material and ions of electrolyte, in the high frequency region. This indicates that both pure pTCAA polymer coated SS electrode material and hetereostructured pTCAA/$TiO_2$ composite electrode materials have acceptable $R_{CT}$ values and good electrical conductivities for practical supercapacitor applications. Due to this easy charge transfer process, there is no remarkable charge accumulation on electrode surfaces and a capacitive behaviour in high frequency region. On the other hand, the Nyquist plots demonstrate shapes of vertical line toward $Z_{RE}$ axis (almost parallel to $Z_{RE}$ axis) by increasing imaginary part ($Z_{IM}$) of the impedance over low frequency region. This electrochemical response is due to diffusion resistance caused by obstruction of ion movements. As ion diffusion resistance rises, penetration of the electrolyte ions toward pores of redox-active electrode materials complicates and a double-layer forms on electrode surfaces. Hereby, redox-active electrode materials begin to behave as an ideal pseudo-capacitor and $C_{spec}$ values are remarkably increased. On the basis of similar electrochemical responses of our PC devices to those described above, it can be said that the pure pTCAA polymer coated and the hetereostructured pTCAA/$TiO_2$ composite redox-active electrode materials showed an ideal pseudo-capacitive behaviour in the low frequency region. Furthermore, impedance measurements revealed synergistic pseudo-capacitive effect of $TiO_2$ redox-active layer. As shown in the Nyquits plots of *Type I*, *Type II* and *Type III* PC devices in **Fig. 5b**, **5c** and 5**d**, respectively, the vertical lines of their Nyquits plots over low frequency region are steeper (or larger slope) compared to *Type IV* reference PC device (**Fig. 5a**). This pronounced difference in Nyquist plots confirmed hetereostructured pTCAA/$TiO_2$ composite redox-active electrode materials have better performances than pure pTCAA polymer coated electrodes and it is compatible with the results obtained from GCD studies.

In addition to charge transfer kinetics and ionic diffusion rates, internal resistance (IR) or equivalent series resistance (ESR) value which is crucial parameter in measuring specific power, was evaluated using Nyquist plots for our PC devices. Internal resistance is total resistance of a pseudo-capacitor device, including the electrolyte resistance, the redox-active material resistance and the contact resistance between active material and current collector. Using the Nyquits plots, internal resistance can be directly determined from the intercept point of the vertical line from low frequency region towards $Z_{RE}$ axis and the $Z_{RE}$ axis. The internal resistance values of 17.56 Ω $cm^2$, 13.57 Ω $cm^2$, 9.71 Ω $cm^2$, 7.75 Ω $cm^2$ were obtained from impedance data for *Type IV, Type III*, *Type II* and *Type I* PC devices, respectively (**Fig. 5a-d**). These values indicated that the integration of different redox-active materials ($TiO_2$ particles and pTCAA conducting polymer layer) reduced significantly internal resistances of electrode materials. More particularly, the impedance data also manifested that the synergistic effect of 3-5 nm sized $TiO_2$ particles more improved not only electronic conductivity, but also electrochemical redox activity of the hetereostructured composite electrode materials more than average 21 nm sized $TiO_2$ and bulk $TiO_2$ particles, since Type I PC device have the lowest internal resistance (IR=7.75 Ω $cm^2$). This obvious performance superiority of the hetereostructured pTCAA/$TiO_2$ (3-5 nm sized) composite electrode material can be attributed to its electronical and morphological properties including: *(i)* 3-5 nm sized $TiO_2$ particles reduced contact resistance , at the interface between the conducting polymer and metal oxide layer, by more strongly

interacting with pendant carboxylic acid groups on pTCAA backbone. The decrease in resistance could enable a more redox-active electrode surface for Faradaic reactions during charge storage process *(ii)* pTCAA/$TiO_2$ (3-5 nm sized) hetereostructured active layer could offer plentiful and efficient diffusion channels or pores for the penetration of ions due to particle size advantage of $TiO_2$ (3-5 nm sized) and thus charge capability highly enhanced.

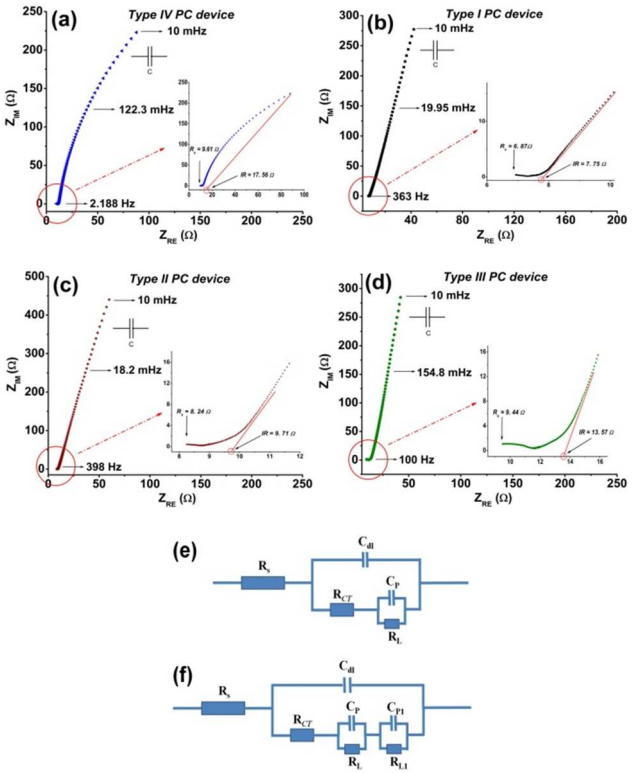


**Fig.5** Nyquits plots for (a) *Type IV* reference PC device (b) *Type I* (c) *Type II* (d) *Type III* symmetric PC devices (insets are corresponding magnified high frequency region) (e) equivalent circuit for *Type IV* reference PC device (f) the equivalent circuit of *Type I, Type II* and *Type III* PC devices

The specific power (SE) values of our PC devices were calculated as 266.96 kW $kg^{-1}$, 202.59 kW $kg^{-1}$ and 138.89 kW $kg^{-1}$ and for *Type I*, *Type II* and *Type III*, respectively, using the following equation:

$$SP = \Delta V^2 / (4x\ m_{ac}\ x\ IR) \qquad (4)$$

where $\Delta V$ is the potential difference (V) (at constant current density of 2.5 mA $cm^{-2}$), $m_{ac}$ is the total mass of active material in the electrodes (mg) and IR is the internal resistance or equivalent series resistance (ESR) obtained from Nyquits plot (Ω).

The equivalent circuit modelling studies were finally performed using impedance data in order to support experimental results. The equivalent circuits for Type IV reference and *Type I*, *Type II* and *Type III* PC devices are represented in **Fig. 5e** and **Fig. 5f.** As can be seen in **Fig 5e**, the equivalent circuit of Type IV PC device comprises of a solution resistance ($R_s$), a charge transfer resistance ($R_{CT}$), a double-layer capacitor ($C_{dl}$) and a pseudo-capacitor ($C_p$) connected in parallel with leakage resistance ($R_L$), just as a typical pseudo-capacitor equivalent circuit. In this equivalent circuit, $R_{CT}$ is connected in parallel with $C_{dl}$ and connected in series with $C_P$. The parallel component configuration of $R_{CT}$ and $C_{dl}$ describes semi-circle response, while $C_P$, which results from conducting polymer redox-active layer, corresponds to vertical line toward $Z_{RE}$ axis in the Nyquits plot (**Fig. 5a**). On the other hand, as seen in **Fig. 5f**, another pseudo-capacitor ($C_{P1}$) as an electrical component is connected in series with the CP in the equivalent circuits of *Type I*, *Type II* and *Type III* PC devices fabricated using hetereostructured pTCAA/$TiO_2$ composite electrode materials. This additional pseudo-capacitor, CP1, is convincing proof of the synergistic pseudo-capacitive effect of $TiO_2$ redox-active layer and it explains the steeper (or large slope) vertical lines in the Nyquits plots of *Type I*, *Type II* and *Type III* PC devices than *Type IV* reference PC device (**Fig. 5 b-d**). The results of theoretical equivalent circuit modelling, are given in **Fig. S13†** (see EIS†), are in good agreement with the experimental impedance data.

## 4. Conclusion

In summary, we have developed a feasible and simple method to fabricated hetereostructured composite electrode material, based on π-conjugated polymer and nano $TiO_2$, for high-performance symmetric supercapacitor applications. The polymeric material, poly(3,6-dithien-2-yl-9H-carbazol-9-yl acetic acid), pTCAA, prepared for the first time, was relevantly designed for the purpose of both creating a strong interaction and potent synergistic pseudo-capacitive effect between conducting polymer layer and nano metal oxide particles. The electrochemical performance tests indicated that pTCAA/$TiO_2$ hetereostructured composite electrode materials present high specific capacitance ($C_{spec}$ = 462.88 F $g^{-1}$), specific energy (SE = 89.98 W h $kg^{-1}$), good cycling performance and high reversible capability (81.7 % capacitance retention), through this unique structural design. The high specific power value or power density (266.96 kW kg-1) denote that our hetereostructured pTCAA/$TiO_2$ composite electrode materials have well potential to be used in many practical or commercial applications that require high power. The results CV, GCD and EIS studies also manifested that particle size of $TiO_2$ has a notable effect on pseudo-capacitive performances of the pTCAA/$TiO_2$ hetereostructured composite electrode materials. pTCAA/$TiO_2$ hetereostructured composite electrode materials were fabricated without using a polymeric binder and conducting additives, unlike most other composite electrodes. Furthermore, pTCAA/$TiO_2$ hetereostructured composite electrodes were used as both anode (p-dopable) and cathode (n-dopable) materials in our solid state PC devices. These key factors also played a significant role in capacitive performances by reducing internal resistance of both hetereostructured composite electrode materials and symmetric solid state PC devices. We believe that a new approach can be readily adapted to prepare novel promising composite electrode materials for advanced high performance supercapacitor applications.

## Acknowledgements

M. Güllü and D. Yiğit are grateful to the Scientific and Technological Research Council of Turkey-TÜBİTAK for their generous financial support (TBAG-110T071). D. Yiğit also thanks TÜBİTAK for postgraduate scholarship.

## Notes and references

[a] *Faculty of Science, Department of Chemistry, Ankara University, Beşevler, 06100, Ankara, Turkey. Fax: +903122232395; Tel: +903122126720, Ext: 1028; E-mail: gullu@ankara.edu.tr*

† Electronic Supplementary Information (ESI) available: $^{1}H$ NMR, $^{13}C$ NMR and MS spectra of novel thiophene derivatives, cyclic voltammogram of monomer (TCAA), shematic representation of symmetric PC device, TEM images of 3-5 nm, 21 nm and bulk sized $TiO_2$ nanoparticles, XRD patterns of composite electrode materials, SEM images of raw SS electrode and $TiO_2$ nanoparticles (3-5 nm sized), Theoretical equivalent circuit models of PC devices. See DOI: 10.1039/b000000x/

1 J. Niv, W. G. Pell and B. E. Conway, *J. Power Sources*, 2005, **156**, 725.
2 P. Simon and Y. Gogotsi, *Nat. Mater*., 2008, **7**, 845.
3 P. Sharma and T. S. Bhatti, *Energy Con. and Manag*., 2010, **51**, 2901.
4 F. Meng and Y. Ding, *Adv. Mater*., 2011, **23**, 4098.
5 B. E. Conway, *Electrochemical Supercapacitors: Scientific Fundamentals and Technological Applications*, Springer, 1998, 698 pages.
6 A. G. Pandolfo and A. F. Hollenkamp, *J. Power Source*, 2006, **157**, 11.
7 K. H. An, W. S. Kim, Y. S. Park, Y. C. Choi, S. M. Lee, D. C. Chung, D. J. Bae, S. C. Lim and Y. H. Lee, *Adv. Mater.*, 2001, **13 (7)**, 497.
8 Q. Jiang, M. Z. Qu, G. M. Zhou, B. L. Zhang and Z. L. Yu, *Mater. Lett*., 2002, **57**, 988.
9 Q. Y. Li, H. Q. Wang, Q. F. Dai, J. H. Yang and Y. L. Zhong, *Solid State Ionics*, 2008, **179**, 269.
10 M. Toyoda, Y. Tani and Y. Soneda, *Carbon*, 2004, **42**, 2833.
11 E. Frackowiak, *Phys. Chem. Chem. Phys*., 2007, **9**, 1774.
12 A. Burke, *J. Power Sources*, 2000, **91 (1)**, 37.
13 W. G. Pell and B. E. Conway, *J. Power Sources*, 2001, **96 (1)**, 57.
14 B. Hsia, M. S. Kim, C. Carraro and R. Maboudian, *J. Mater. Chem. A*., 2013, **1**, 10518.
15 L. L. Zhang and X. S. Zhao, *Chem. Soc. Rev*., 2009, **38**, 2520.
16 K. R. Prasad and M. Munichandraiah, *J. Power Sources*, 2002, **112**, 443.
17 M. M. Khandpekar, R. K. Kushwaka and S. P. Pati, *Solid-State Elect*., 2011, **62**, 156.
18 F. Marchioni, J. Yang, W. Walker and F. Wudl, *J. Phys. Chem. B*, 2006, **110**, 22202.
19 C. Arbizzani, M. C. Gallazzi, M. Mastragstina, M. Rossi and F. Soavi, *Electrochemistry Commun*. 2001, **3**, 16.
20 P. Soudan, P. Lucas, H. A. Ho, D. Jobin, L. Breau and D. Belanger, *J. Mater. Chem*., 2001, **11**, 773.
21 C. Arbizzani, M. Mastragstina and L. Meneghello, *Electrochim. Acta*, 1996, **41 (1),** 21.
22 D. Y. Liu and J. R. Reynolds, *Applied Materials & Interfaces*, 2010, **2 (12)**, 3586.
23 C. C. Hu, Y. H. Huang and K. H. Chang, *J. Power Sources*, 2002, **108**, 117.
24 U. M. Patil, R. R. Salunkhe, K. V. Gurav and C. D. Lokhande, *Appl. Surf. Sci.*, 2008, **255**, 2603.
25 X. Zhou, H. Chen, D. Shu and C. He, *J. Phys. Chem. Solids*, 2009, **70**, 495.
26 Y. R. Ahn, M. Y. Sang, S. M. Jo and C. R. Park, *Nanotechnology*, 2006, **17**, 2865.
27 J. Yan, T. Wei, J. Cheng, Z. Fan and M. Zhang, *Mater. Res. Bull*., 2010, **45**, 210.
28 N. Miura, S. Oonishi and K. Rajendra, *Electrochem. Solid-State Lett*., 2004, **7**, 5540.
29 M. Nakayama, A. Tanaka and Y. Sato, *Langmuir*, 2005, **21**, 5907.
30 C. C. Chein, P. C. Chen, J. Zou and S. J. Hsieh, *Advanced Materials Research*, 2012, **535-537**, 894.
31 H. Lee, M. S. Cho, I. H. Kim, J. D. Nam and Y. Lee, *Synthe. Met*., 2010, **160**, 1055.
32 J. P. Zheng, P. J. Cygan and T. R. Jow, *J. Electrochem. Soc*., 1995, **142**, 2699.
33 Y. Zhang, H. Ding and M. Zhang, *Thin Solid Films*, 2008, **516**, 7381.
34 W. Sugimoto, H. Iwata, K. Yokoshima, Y. Murakami and Y. Takasu, *J. Phys. Chem. B*, 2005, **109**, 7330.
35 L. Fan and J. Maier, *Electrochem. Commun*., 2006, **8**, 937.
36 K. R. Prased, K. Koga and N. Miura, *Chem. Mater*., 2004, **16**, 1843.
37 Y. Zhau, B. He, W. Zhou, J. Huang, X. Li, B. Wu and H. Li, *Electrochim. Acta*, 2004, **49**, 257.
38 M. Kaloji, P. J. Murphy and G. O. Williams, *Synthe. Met*., 1999, **102**, 1360.
39 V. Gupta and N. Miura, *Mater. Lett*., 2006, **60**, 1466.
40 R. K. Sharma, A. C. Rastogi and S. B. Desu, *Electrochim. Acta*, 2008, **53**, 7690.
41 G. D. Snook, P. Kao and A. S. Best, *J. Power Sources*, 2011, **196**, 1.
42 Y. Zhang and Z. Qin, *Integr. Ferroelectrics*, 2011, **128**, 86.
43 S. H. Mujawar, S. B. Ambade, T. Battumur, R. B. Ambade and S. Lee, *Electrochim. Acta*, 2011, **56**, 4462.
44 J. P. Ferraris, M. M. Eissa, I. D. Brotherston and D. C. Loveday, *Chem. Mater*., 1998, **10**, 3528.
45 K. S. Ryu, Y. G. Lee, Y. S. Hang, Y. J. Park, X. Wu, K. M. Kim, M. G. Kang, N. G. Park and S. H. Chang, *Electrochim. Acta*, 2004, **50**, 843.
46 J. H. Huang and C. W. Chu, *Electrochim. Acta*, 2011, **56**, 7228.
47 Y. Armel, J. Rivnay, G. Mallianas and B. W. Jensen, *J. Am. Chem. Soc*., 2013, **135**, 11309.
48 D. Yiğit, T. Güngör and M. Güllü, *Organic Electronics*, 2013, **14**, 3249.
49 E. Ermiş, D. Yiğit and M. Güllü, *Electrochim. Acta*, 2013, **90**, 623.
50 S. A. Hashmi and H. M. Upadhyaya, *Ionics*, 2002, **8 (3-4)**, 272.
51 Z. A. Hu, Y. L. Wang, Y. X. Ma, L. P. Yang and Y. Y. Zhang, *Mater. Chem. and Phys*., 2009, **114 (2-3)**, 990.
52 W. F. Mak, G. Wee, V. Anavindan, N. Gupta, S. G. Mhaisalkar and S. Madhavi, *J. Electrochem. Soc*., 2012, **154 (2),** A1481.
53 P. Sen and A. De, *Electrochim. Acta*, 2010, **55**, 4677.
54 R. K. Sharma and L. Zhai, *Electrochim. Acta*, 2009, **54**, 7148.
55 L. Zhang, X. Wang, H. An, X. Wang, L. Yi and L. Bai, *J. Solid State Electrochem*., 2011, **15**, 675.
56 T. T. Tung, T. Y. Kim, J. P. Shim, W. S. Yang, H. Kim, K. S. Suh, *Organic Electronics*, 2011, **12**, 2215.
57 R. Liu, J. Duay, T. Lane and S. B. Lee, *Phys. Chem. Chem. Phys*., 2010, **12**, 4309.
58 C. Bian, A. Yu and H. W, *Electrochem. Com*., 2009, **11**, 266.
59 W. Chen, Y. He, X. Li, J. Zhou, Z. Zhang, C. Zhao, C. Gang, S. Li, X. Pan and E. Xie, *Nanoscale*, 2013, **5**, 11733.
60 D. Zhang, Q. Q. Dong, X. Wang, W. Yan, W. Deng and L. Y. Shi, *J. Phys. Chem. C*., 2013, **117**, 20446.
61 A. J. Roberts and R. C. T. Slade, *Electrochim. Acta*, 2010, **55**, 7460.
62 S. Radhakrishnan, C. R. K. Rao and M. Vijayan, *J. Appl. Polymer Science*, 2011, **122**, 1510.
63 M. M. Khandpekar, R. K. Kushwaha, S. P. Pati, *Solid-State Electronics*, 2011, **62**, 156.
64 N. Bertan, I. F. Francke, D. Bourrat, F. Chandezan and S. Sadki, *J. Phys. Chem. B*, 2009, **113**, 14087.
65 E. Emregül, Ö. Kocabay, B. Derkus, T. Yumak, K. C. Emregül, A. Sınağ and K. Polat, *Bioelectrochemistry*, 2013, **90**, 8.
66 V. Promarak and S. Ruchirawat, *Tetrahedron,* 2007, **63**, 1602.
67 J. Cabaj, K. Idzik, J. Soloducha and A. Chyla, *Tetrahedron*, 2006, **62**, 758.
68 B. Hu, Y. Zhang, X. Lv, M. Ouyang, Z. Fu and C. Zhang, *J. Electroanal. Chem.*, 2013, **689**, 291.

69 S. G. Pawar, S. L. Patil, M. A. Chougule, B. T. Raut, S. Sen and V. B. Patil, *Inter. Journal Polym. Mater.*, 2011, **60**, 979.
70 E. C. Landis, S. C. Jensen, K. R. Phillips and C. M. Friend, *J. Phys. Chem.*, 2013, DOI: org10.1021/jp308784q.
71 A. Ramadoss, G. S. Kim and S. J. Kim, *Cryst. Eng. Comm*., 2013, **15**, 10222.
72 F. E. Amitha, A. L. M. Reddy and S. Ramaprabhu, *J. Nanopart. Res*., 2009, **11**, 725.
73 Z. Zhang, F. Xiao, Y. Guo, S. Wang and Y. Liu, *ACS. App. Mater. Interfaces*, 2013, **5**, 2227.
74 X. Sun, M. Xie, G. Wang, H. Sun, A. S. Cavanagh, J. J. Travis, S. M. George and J. Lion, *J. Electrochem. Soc.,* 2012, **159 (4)**, A364.
75 M. Selvakumar and D. K. Bhat, *App. Surface Sci*., 2012, **263**, 236.
76 Q. Tan, Y. Xu, J. Yang, L. Qiu, Y. Chen and X. Chen, *Electrochimica Acta*, 2013, **88**, 526.
77 A. Ramadoss and S. J. Kim, *Carbon*, 2013, **63**, 434.

Table of contents entry

Graphical abstract

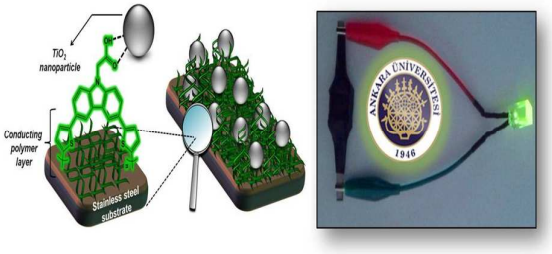


Textual abstract

The hetereostructured composite electrodes exhibited specific capacitance ($C_{spec}$= 462.88 F $g^{-1}$), specific power (SP= 266.96 kW $kg^{-1}$), specific energy (SE= 89.98 Wh $kg^{-1}$), good cycling performance and excellent reversible capability.